ELSEVIER

Biophysical Chemistry 78 (1999) 259–269

Biophysical Chemistry

Structural and dynamical properties of two DNA oligomers with the same base composition and different sequence

F. Barone[a], M. Matzeu[a], F. Mazzei[a,*], F. Pedone[b]

[a] *Laboratorio di Fisica, Istituto Superiore di Sanità, Viale Regina Elena 299, 00161 Roma, Italy*
[b] *INFM, Università 'La Sapienza', Roma, Italy*

Received 2 December 1998; received in revised form 18 February 1999; accepted 18 February 1999

Abstract

We compared the structural and dynamical properties of two DNA fragments, 27 bp long, having the same base composition but a different sequence. This work aims to understand how the base sequence on a purine rich strand in a double helix, which is important for many biological functions, is related to structural features and to measurable physical quantities. Structural characterization of the two samples was performed both by conventional spectroscopic methods (circular dichroism and UV denaturation experiments) and by means of a γ-ray footprinting technique which gives information on fine conformational differences. Dynamical features of the samples were studied by fluorescence polarization anisotropy (FPA) measurements which allow the evaluation of some hydrodynamic parameters, such as the hydrodynamic radius and the elastic torsion constant of DNA. Using a γ-ray footprinting technique, we observed that the interruption of the long homopurine–homopyrimidine run in the control sample, due to the 'scrambling' operation, alters the DNA three-dimensional structure, also at nucleotide level. Besides, an increase in thermal stability and in the torsional rigidity of the 'scrambled' sample was observed. A possible association between base-stacking interaction and torsional rigidity was inferred from the comparison of the two samples. © 1999 Elsevier Science B.V. All rights reserved.

Keywords: DNA structure; FPA; DNA dynamics

1. Introduction

An increasing number of data supports the notion that the sequence of DNA is reflected in its conformation [1]. Often, the sequence-specific conformation is relevant in intermolecular recognition processes, such as the interaction of curved DNA structures with promoters [2] or of Z DNA with specific antibodies [3]. These findings have stimulated research in this field, relying on the availability of new sophisticated technologies and

* Corresponding author. e-mail: mazzei@iss.it

0301-4622/99/$ - see front matter © 1999 Elsevier Science B.V. All rights reserved.
PII: S0301-4622(99)00026-5

of synthetic oligonucleotides of required length and sequence. Different classes of DNA conformations are shown in the Nucleic Acid Data base (NDB) [1] and recent structural refinements reveal new insight into sequence-dependent DNA structure [4].

Perhaps a lack of knowledge exists regarding two main points. The first one is related to the dimensions of the oligomers, generally studied by X-ray crystallography or NMR techniques, since they cannot be longer than 12 bp. The second one concerns the study of DNA dynamics and its relations with base sequence and structural features. Only recently have dynamical measurements been performed on well characterized DNA fragments, using ethidium bromide (EB) as fluorescent probe [5–8]. We want to understand to what extent the DNA sequence influences its internal motion, expressed by bending and twisting of the double helix. Otherwise put, we investigate the 'deformability' of DNA tracts, which might influence the association with proteins or nucleic acid strands, as in triplex formation.

In this paper, the effect of mixing some base pairs in a 27-mer DNA fragment both on its structural and dynamical properties was studied. The control sample, already characterized in a previous work [8], contained a 21-bp long homopurinic tract in a central position. We investigated this particular sequence since long runs of purines are known to be involved in gene regulation in eucaryotes and are recognized to have a functional role in biological processes: recently, the interest in sequences containing long purine tracts has been renewed because of their possible use in gene therapy, through the formation of a triple helix [9]. We removed the long 21 homopurine–homopyrimidine run present in the control sample, by a 'scrambling' operation. In particular the six pyrimidines located at the end terminals were interspersed in the 21 long purine run. Furthermore, we took care of avoiding the recurrence of more than two consecutive adenines along a strand, which are associated with the appearance of a more complex DNA structure.

We used the γ-ray footprinting technique [10,11], in order to explore the three-dimensional fine arrangement of the phosphodiester backbone. We also applied conventional spectroscopic methods to study global conformation and thermal stability in the two samples. Finally, we performed fluorescence polarization anisotropy decay (FPA) measurements in order to evaluate the hydrodynamic radius and the elastic torsion constant [5–8].

2. Material and methods

2.1. DNA fragment preparation

Oligonucleotides were purchased from M-Medical Genenco and length homogeneity was checked by denaturing gel electrophoresis. As a rule, the fraction of shorter contaminating fragments was less than 3%. For purification, single strand oligonucleotides were run on 20% polyacrylamide denaturing gels [12]. Bands, visualized by UV radiation using silica plates, were excised and eluted by an overnight incubation in deionized water.

The concentration of single strands was determined spectrophotometrically with molar extinction coefficients calculated by using nearest-neighbour analysis [13]: $\epsilon_1 = 2.23 \times 10^5$ M^{-1} cm^{-1}, $\epsilon_2 = 3.02 \times 10^5$ M^{-1} cm^{-1}, $\epsilon_3 = 2.24 \times 10^5$ M^{-1} cm^{-1}, $\epsilon_4 = 3.05 \times 10^5$ M^{-1} cm^{-1}. In order to obtain the samples shown in Fig. 1a, oligonucleotides (1) and (2) (control duplex) and (3) and (4) ('scrambled' duplex) were mixed in the proper ratio in 10 mM sodium phosphate buffer (pH 6.1). Annealing was performed by heating at 80°C for 10 min and letting the samples cool down to 4°C over a 16–18-h period. The purity grade of our duplex samples was checked by 15% polyacrylamide gel analysis in non-denaturing conditions [45 mM Tris-Borate, 1 mM Na_2EDTA (TBE buffer), pH 8] run at 4°C for 17 h (Fig. 1b).

2.2. Circular dichroism measurements

Circular dichroism (CD) measurements were performed by means of a Jasco J710 spectropolarimeter. Spectra were recorded between 320 and 220 nm with a scanning rate of 10 nm min^{-1}. The spectral resolution was 0.2 nm and the band width 1 nm. The samples, dissolved in 10 mM phos-

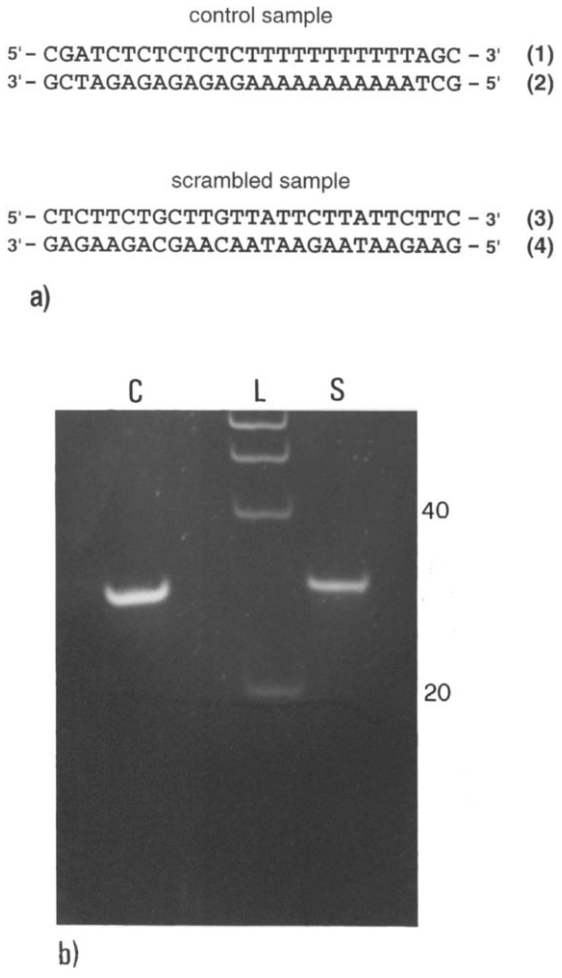

Fig. 1. (a) Secondary structure of duplex oligonucleotides: control sample containing a long purine sequence and DNA fragment with 'scrambled' sequence; (b) polyacrylamide gel electrophoresis of the two samples. C, control; L, 20-bp ladder (from GenSura, Biotech, Italy); S, 'scrambled' sample.

phate buffer, pH 6.1 (TP buffer) were placed in a cylindrical water-jacketed cell (1-cm path length) and thermostated at 10°C by means of a Haake H20 bath.

2.3. Ultraviolet absorption denaturation curves

The absorbance changes as a function of temperature were recorded with a Cary 3 UV/VIS spectrophotometer. The samples, usually at a concentration of 50 μg ml^{-1} in TP buffer, were thermostated using a Peltier device. The temperature was raised at a rate of 0.5°C min^{-1} and data points recorded every 0.2°C. Absorbance values were corrected for thermal expansion of the water and normalized at $A_{260} = 1$ at the lower temperature.

Thermodynamic analysis was based on a two-state model for duplex–single strand transitions, by using generalized equations [14]. In the model, the equilibrium constant K of the transition is expressed in terms of the fraction of single strands in the duplex state ($\alpha_m = 0.5$ at the melting point), of the molecularity of the reactions ($n = 2$) and of the total strand concentration C_T. The fraction α_m was calculated by subtracting sloping baselines. Values of van't Hoff enthalpy and Gibbs free energy differences were calculated from the equations as follows:

$$\Delta H_{VH} = (2 + 2n)RT_m^2\left(\frac{\mathrm{d}\alpha_m}{\mathrm{d}T}\right)_{T_m}$$

$$\Delta G(T) = -RT \ln K(T)$$

2.4. γ-ray footprinting

Single stranded purine rich oligomers were 3′-end labeled by incubation with [α-^{32}P]ddATP (Amersham) and the terminal transferase enzyme (Boehringer, Mannheim, Germany) and then further purified on a Sephadex G-25 column. Annealing of the 3′ end-labeled oligomer with an excess of unlabeled complementary strand was performed in 10 mM sodium phosphate buffer (pH 6.1). Labeled samples, dissolved in 100 μl of buffer were irradiated, on an ice bath, in a GammaCell 220 (AECL), equipped with a ^{60}Co source, at the dose of 180 Gy. The dose rate was approximately 6.1 Gy min^{-1}.

Irradiated samples were electrophoresed at high voltage on 20% denaturing polyacrylamide gels ($20 \times 40 \times 0.04$ cm), containing 7 M urea in TBE, as described by Sambrook et al. [12]. Gels were run at 27 W, fixed for 10 min in 10% acetic acid, dried at 60°C and autoradiographed using Kodak X-OMAT S films and a Kodak X-OMATIC cassette with intensifying screens. To achieve a bet-

ter resolution of the bands, two gels were run for each sample: the first one for 2 h and the second one for 4 h (short- and long-run, respectively). The densitometric analysis of autoradiographs was performed by an ULTROSCAN XL (Pharmacia LKB) laser densitometer. The area of each band was evaluated using the public domain NIH Image program (developed at the US National Institute of Health and available on the Internet at http://rsb.info.gov./nih-image/). The area values were normalized at the total area of the measured bands.

2.5. Dynamic fluorescence measurements

Lifetime and Fluorescence Polarization Anisotropy measurements were performed on a K2-ISS phase-shift fluorometer instrument (Urbana IL, USA) using the 514-nm 0.5-W output of a Coherent Innova 90C Argon laser. The modulation ratio of the excitation light was always in the range 60–70% and the detection cross-correlation frequency was 80 Hz.

Samples were placed into 1-cm quartz cells and a long-pass filter (550 nm) was set between the sample turret and the photomultiplier to minimize detection of scattered light. For lifetime measurements, 10 frequencies logarithmically spaced in the 2–40-MHz interval were acquired. The excitation polarizer was set at 35° and polystyrene lattice was used as reference.

For FPA measurements, 20 frequencies were acquired in the 2–40-MHz interval the excitation polarizer being fixed at 0° (i.e. vertical) and the emission polarizer automatically rotated at 0 and 90° for each acquisition. The differences between phase shifts and the ratios between the modulation ratios measured for the two relative positions of the polarizer and the analyzer characterize the fluorescence anisotropy as discussed in Section 2.6. The error for the phase and modulation was 0.2 and 0.004°, respectively, amounting to $\cong 1\%$ of the signal. The temperature of the samples was controlled by means of a circulating water bath (Haake K15) and kept constant at 10°C. The DNA samples were dissolved in 10 mM sodium phosphate (pH 6.1) buffer and 200 mM NaCl. Ethidium bromide (2,7-diamino-10-ethyl-9-phenylphenanthridinium bromide) was from Boehringer and it was dissolved in the same buffer at a fixed concentration of approximately 1 μM.

To avoid energy transfer processes among intercalated dye molecules, the DNA base pairs/EB ratio was usually greater than 200.

Data were analyzed with the ISS fluorometer software for lifetimes determination and with a Vax for the anisotropies.

2.6. Theory

The computation of the fluorescence anisotropy decay for a realistic DNA model has been given by Allison and Schurr [15]; this model has been adapted for phase fluorometry by Collini et al. [6]. In general, the fluorescence anisotropy $r(t)$ is given by products [5] of internal geometric factors $A_n(t)$, due to the particular dye intercalating geometry, and of bending $F_n(t)$ and torsional $C_n(t)$ correlation functions:

$$r(t) = \frac{(I_{\parallel} - I_{\perp})}{(I_{\parallel} + 2I_{\perp})} = r_0 \sum_{n=-2}^{2} A_n(t) C_n(t) F_n(t) \tag{1}$$

where $I_{\parallel}$ and $I_{\perp}$ are the fluorescence intensities measured with the polarizer oriented in parallel and in perpendicular position, respectively, r_0 is the initial anisotropy value, assumed to be 0.36 due to the isotropic dye wobbling. The internal correlation functions $A_n(t)$ are related to the angle θ formed by the EB dipole and the helix axis, assumed to be 70.5° [5]:

$$A_0 = \left(\frac{3}{2}\cos^2\vartheta - \frac{1}{2}\right)^2;$$

$$A_1 = 3\cos^2\vartheta \sin^2\vartheta\,;\; A_2 = \frac{3}{4}\sin^4\vartheta$$

The torsional correlation functions $C_n(t)$ are related to the relaxation time τ_l of the lth normal

mode and to its corresponding mean square amplitude d_l^2 by:

$$C_n(t) = (N+1)^{-1}\exp\left(-n^2 D_{\|} t\right) \times \sum_{m=1}^{N+1} \exp\left[-n^2 \sum_{l=2}^{N+1} d_l^2 Q_{ml}^2 (1 - e^{-t/\tau_l})\right] \quad (2)$$

where Q_{ml} is the element of the normal mode transformation matrix associated with the lth normal mode and to the mth subunit as reported by Schurr [5], N is the number of base pairs and D is the rotational diffusion coefficient. These quantities are given by:

$$\tau_l = \frac{\gamma}{4\alpha \sin^2[(l-1)\pi/[2(N+1)]]};$$

$$d_l^2 = \frac{k_B T}{4\alpha \sin^2[(l-1)\pi/[2(N+1)]]};$$

$$Q_{ml} = [2/(N+1)]^{1/2} \cos\left[\left(m - \frac{1}{2}\right) \times (l-1)\pi/(N+1)\right]; \gamma = \frac{k_B T}{D_{\|}(N+1)}$$

where α is the DNA torsional constant which is related to the torsional rigidity C and to the base pair height $b = [L/(N+1)]$ through $\alpha = C/b$ and γ is the rotational friction coefficient.

For a straight fragment, the rotational diffusion coefficients can be computed by assuming that the DNA behaves as a straight cylinder of length L and radius R, i.e. [16]:

$$D_{\|} = k_B T/\left[(3.8441)\pi\eta L R^2 (1 + \delta_{\|})\right];$$

$$D_{\perp} = 3k_B T(\ln p + \delta_{\perp})/\pi\eta L^3 \quad (3)$$

$$\delta_{\|} = (0.677/p) - (0.183/p^2);$$

$$\delta_{\perp} = -0.662 + (0.917/p) - 0.05/p^2$$

where $p = (L/2R)$, T is the absolute temperature and η is the solution viscosity.

The bending correlation functions $F_n(t)$ are expressed according to:

$$F_n(t) = \exp\left[-(6-n^2) D_{\perp} t\right] \cdot \exp\left[-(6-n^2) A_n \sum_{k=l}^{k_{max}} \frac{(1 - e^{-t/T_k})}{(2k+1)^2}\right] \quad (4)$$

where

$$A_n = \frac{-\ln D_n(\infty)}{\left[(6-n^2) \sum_{k=1}^{k_{max}} \frac{1}{(2k+1)^2}\right]}$$

and

$$D_n(\infty) = (Z_n)^{-1/2} \exp(-Z_n/3)(\pi^{1/2}/2)\mathrm{erf}(Z_n^{1/2})$$

and $Z_n = (6-n^2)L/4P$; erf is the error function.

$$\frac{1}{T_k} = \frac{k_B T P k_k^4}{4\pi\eta}\left[K_0(k_k R_H) + \left(\frac{k_k R_H}{2}\right) K_1(k_k R_H)\right]$$

and

$$k_k = \frac{(2k+1)\pi}{2L}$$

The maximum number of relaxation bending modes, k_{max}, was chosen as the index k for which $T_{k+1} > T_k$ and was typically equal to 10. The dynamic persistence length P was computed from the bending rigidity A according to: $P = A/(KT)$.

The Laplace transform of the time decay of the fluorescence intensity as measured when the relative orientation of the excitation polarizer and the emission analyzer are parallel, $I_{\|}(t) = I_{tot}(t)(1 + 2r(t))$, and orthogonal, $I_{\perp}(t) = I_{tot}(t)(1 - r(t))$ are:

$$f_p(\omega) = \int_0^{\infty} dt I_p(t) e^{i\omega t} = L(I_p)(i\omega) \quad (8)$$

where $p = \|$ or $p = \perp$ were computed and combined as fluorescence phase shift differences $\Delta(\omega)$ and demodulation ratios $\Lambda(\omega)$

$$tg(\Delta(\omega)) = \frac{\mathrm{Im}(f_\perp)\mathrm{Re}(f_\|) - \mathrm{Re}(f_\perp)\mathrm{Im}(f_\|)}{\mathrm{Re}(f_\perp)\mathrm{Re}(f_\|) + \mathrm{Im}(f_\perp)\mathrm{Im}(f_\|)}$$

$$\Lambda(\omega) = |f_\perp(\omega)|/|f_\|(\omega)| \quad (9)$$

The Laplace transform of Schurr's model was computed (Eqs. (1), (2) and (4)) with a numerical Fast Fourier Transform procedure.

3. Results

3.1. Circular dichroism spectra and UV melting curves

Fig. 2 shows the circular dichroism spectra of duplex samples at 10°C. In the control duplex the sharp shoulder at approximately 260 nm, characteristic of poly(dA)poly(dT) and of A tracts containing DNAs [17] is evident. It is interpreted as due to the particular conformation, characterized by high propeller twist (B_p conformation), stabilized by cross-strand hydrogen bonds between adenine N_6 and thymine 0_4 [18,19]. This shoulder is not present in the circular dichroism spectrum of the 'scrambled' sample whose sequences never contain more than two consecutive adenines. Furthermore, in this last sample we observe a greater ellipticity and a shift of the maximum towards lower wavelengths. There are no differences in the intensity of the negative band at approximately 250 nm.

In Fig. 3 derivative melting curves of the two samples are shown. The 'scrambled' duplex exhibits a greater stability as to the control one, as pointed out by the melting temperatures and the $\Delta G_{25°}$ values. The values corresponding to the control samples were $T_m = 40.1 \pm 0.5$°C, $\Delta G_{25} = 16.1 \pm 1.6$ kcal mol^{-1}, while the 'scrambled' sample had $T_m = 43.6 \pm 0.5$°C and $\Delta G_{25°} = 20.8 \pm 2.0$ kcal mol^{-1}. The enthalpy changes due to the transition, as calculated from derivative curve shapes of Fig. 3, are $\Delta H = 167 \pm 17$ kcal mol^{-1} and $\Delta H = 227 \pm 22$ kcal mol^{-1}, respectively. The cooperativity of the melting transitions can be deduced taking into account the value of

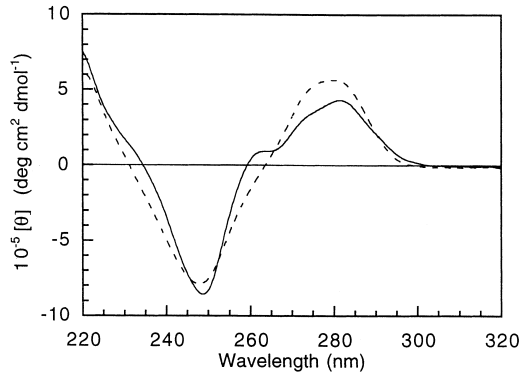

Fig. 2. Circular dichroism spectra of 27-mer DNAs, at 10°C. Solid line, control sample; dashed line, 'scrambled' sequence.

$(\mathrm{d}A/\mathrm{d}T)_m$ at the melting point (proportional to ΔH) in addition to the width of the peak at half height ($l_{1/2}$) and to the difference between the temperature at which the fraction of denatured molecules is equal to 0.5 ($T_{1/2}$) and that of the maximum of the derivative value (T_m). We obtain for the control and 'scrambled' sample, respectively: $(\mathrm{d}A/\mathrm{d}T)_m = 0.136$ and $0.175°\mathrm{C}^{-1}$, $l_{1/2} = 4.5$ and 3.9°C, $T_m - T_{1/2} = 1.5$ and 0.5°C. These values are indicative of a depression of cooperativity during the dissociation of the control with respect to the scrambled sample.

3.2. γ-ray footprinting

Hydroxyl radicals produced by water radiolysis have been shown to be particularly useful in

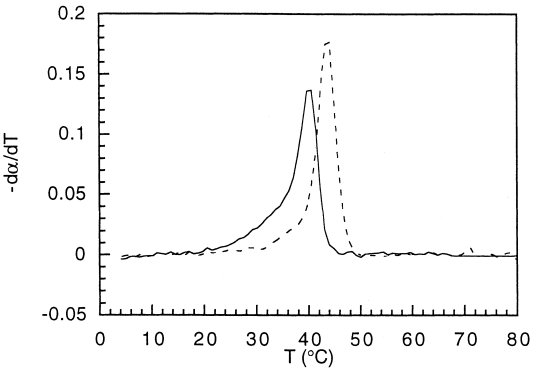

Fig. 3. Derivative melting profiles of the DNA oligomers. Solid line, control sample; dashed line, 'scrambled' sequence.

detecting fine structural features of nucleic acids conformation [20,10,11]. The small dimension of the probe enabled us to reveal differences in the DNA structure at nucleotide level. The OH radicals interact and cleave the sugar phosphate backbone by extracting a hydrogen atom, preferentially at the C4′ and C5′ positions [21] in the minor groove of the double helix.

As compared with the chemical footprinting, this method has the advantage in that it can be used without any further addition of chemicals or enzymes, so that γ-ray footprinting is quite representative of the true molecule conformation.

In Fig. 4a,b the gel autoradiographs of the irradiated samples are shown. In Fig. 5a,b we report the cutting frequency distribution of the

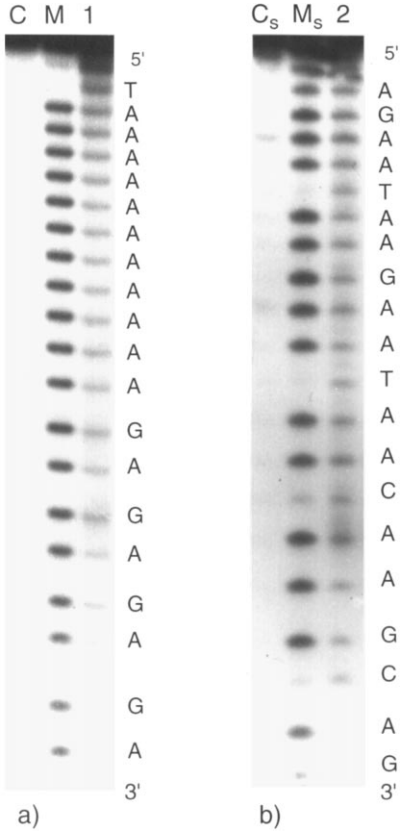

Fig. 4. Autoradiographs of the long-run gel (see Section 2). (a) Control sample; (b) 'scambled' sample. C and Cs, unirradiated samples; M and Ms, sequence markers for guanine and adenine performed according to [22]; 1 and 2, irradiated samples.

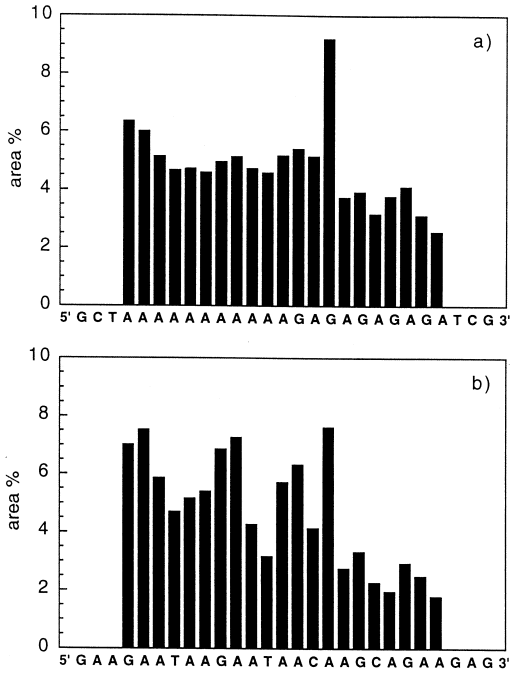

Fig. 5. γ-ray footprinting data analysis. (a) Control sample; (b) 'scrambled' sample.

studied sequences, where the pattern relative to three bases at the 5′ and 3′ ends has been omitted (see Section 2). The area calculation at these sites was not possible for the poor resolution of the bands in the upper part of the gel and the very limited intensity of the bands in the lower part of the gel, as shown in Fig. 4.

The control sample contains an 11-mer dA repeat in the long purinic tract. This structural feature is reflected in the profile shown in Fig. 4a, where an almost homogeneous cutting frequency is observed. At the G17 position, near the boundary of the poly(dA_{11}) tract, the cutting frequency is almost twice the average. The homogeneity of the radiosensitivity of the poly(dA_{11}) region might stem from the constancy of the minor groove width, according to the data of Crothers [23] and of our previous results [11], and from the presence of a regular hydration spine, that is usually found in dAdT regions [24,25]. It must be remembered that the rate of OH radical attack depends on water diffusion inside the DNA minor groove.

As a result of the 'scrambling' operation of the DNA control sequence, we observe a large modification of the γ-ray footprinting pattern with the disappearance of the almost regular cutting pattern of the long dAdT region.

In the cleavage pattern of the scrambled oligomer (Fig. 5b) two very similar patterns of radiosensitivity, due to the same sequence GAATAA, are evident. In the region of the fragment toward the 3′ end a decrease in the mean cutting frequency is observed.

3.3. Fluorescence polarization anisotropy measurements

FPA data analysis of DNA oligomers assumes that these molecules behave as cylindrical rods subjected to twisting, tumbling and bending motions. Whilst the latter two give poor information in short samples, as in our case, the twisting motion allows derivation of the torsional elastic constant (α) between adjacent base pairs. This is the most suitable parameter, related to local structure, for characterizing the influence of the sequence on the dynamics of DNA molecules.

In Fig. 6a,b the measured values, at 10°C, of demodulation ratios and phase difference of the control and 'scrambled' sample, respectively, are reported, as a function of the modulation frequency. Some differences are evident between the two samples in the figure. These differences are better estimated looking at the parameters, reported in Table 1, and evaluated following the procedures already described in the Section 2. In this table the hydrodynamic radius (R_H) and the torsional constant (α) are reported together with the respective lifetimes of the intercalated and free EB. Good χ^2 values were obtained in the anisotropy data fitting procedures and are reported in Table 1. A major difference is observed between the alpha values of the two samples, where the presence of the long purine tract (control sample) reduces the rigidity of DNA. A slight difference is also evident in the hydrodynamic radius; the control sample exhibits a 0.8 Å increase in the hydration shell diameter.

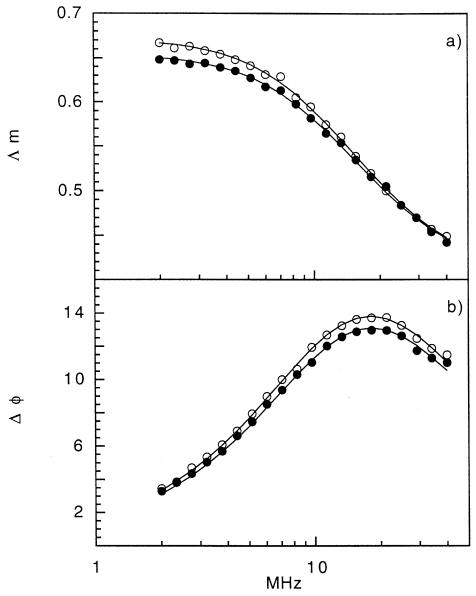

Fig. 6. FPA experimental data for the two 27-bp DNA fragments, at 10°C. Demodulation ratios (a) and phase differences (b) are shown as a function of the modulation frequency. (o) control sample; (●) 'scrambled' sample. Solid lines represent analytical best fits of the data, obtained according to Schurr [5].

Table 1
Hydrodynamic parameters derived from FPA measurements at 10°C

Sample	$\alpha \times 10^{-12}$ erg	R_H (Å)	τ_b (ns)
Control	4.2 ± 0.2	11.1 ± 0.3	21.7 ± 0.5
Scrambled	4.7 ± 0.2	10.7 ± 0.3	23.1 ± 0.5

Data fit was performed according to Allison and Schurr [15], with $r_o = 0.36$ and $A = 8.22$. The lifetime of the free EB was 1.7 ns. The χ^2 value for obtaining α and R_H was approximately 1.1 for both samples.

4. Discussion and conclusion

Up to now, the fine details of DNA structure have been revealed and well described only for very short fragments, 10–12 bp long. A rich data base is now available (NDB data base) and a possible correlation between sequence and structure might be observed. The analysis of longer DNA molecules has been hindered by the objective difficulty in obtaining crystals for X-ray

diffraction studies or in studying them by nuclear magnetic resonance.

Longer DNA molecules are usually better characterized on the basis of average parameters, related to the global conformation or to their thermodynamic properties, while, as far as their fine structure is concerned, their characteristics are generally hypothesized to be analogous to those observed in the 10–12 mer fragments of similar sequence.

In this study we attempt to partially overcome this 'gap' and analyze two DNA fragments, both 27 bp long and with the same base composition but with different sequences, both from a macroscopic and a microscopic point of view. Their properties were always studied in buffer solution.

All the properties of the two fragments gave quite different results. Overall conformation features were defined by studying them with circular dichroism, while their structure, being differently accessible to the hydroxyl radical attack, revealed subtle differences in the backbone arrangement in the two cases. Finally, some internal dynamics properties were revealed by the decay of fluorescence polarization, which is mainly due to rotational (torsional) motions for fragments of this length.

γ-ray footprinting analysis distinguishes well molecular features of the two samples. The presence of a long run of dA produced the appearance of a homogeneous surface, while a fine modulation of the cutting pattern was observed in the sample whose bases were randomly mixed. Besides, a general decrease in accessibility of the hydroxyl radicals was observed in the 'scrambled' sample. The observed effects, easily related to base sequence, are due to a fine difference in local conformation and they could also be related to the presence of an hydration spine which influences the accessibility of OH radicals.

In particular, we confirm the opportunity of using this method to study the three-dimensional arrangement of DNA molecules in solution, also for fragments longer than a dozen base pairs. In a previous paper [11] we noticed that in DNA molecules, containing repeated short runs of dA deoxynucleotides, a narrowing of the minor groove could be detected, while for A-tracts longer than 6 bp a uniform cutting pattern was observed. Now again, the association between a cutting pattern modulation and a narrowing of the DNA minor groove might be inferred. In particular, we refer to the AAT region, also contained in the central part of the Dickerson dodecamer [26], whose structure is characterized by a reduced minor groove width, as established by X-ray crystallography. In the 'scrambled' sequence the two adjacent repeated GAATAA sequences show the same cutting pattern. Further analysis will be required to verify if this property is confirmed when the sequence is located in a different environment. Notwithstanding the fine differences in the backbone, the overall DNA conformation still resembles that of a B-DNA in both cases. However, the presence of the dA_{11} tract is very well detectable from CD spectra, as shown from the characteristic shoulder position of the CD positive band.

The rearrangement of the base pair sequence produces a small increase in thermal stability, as observed by melting denaturation experiments. As hydrogen bonds participate equally in the stability of the two oligomers, two different stacking interactions have to be involved in the different thermodynamical behaviors. Calculations of nearest-neighbour free energy can be carried out according to many authors [14,27,28]. The comparison between ΔG values of the two samples, calculated by taking into account nearest neighbour values (data not shown), does not reveal significant differences in the stability of the two samples. Possibly, interactions beyond nearest-neighbour bases should be taken into account in theoretical previsions, in order to correlate them with our results.

From anisotropy polarization fluorescence experiments an increased rigidity was observed in the 'scrambled' sample together with a little decrease in the hydrodynamic radius. Both parameters are in the range of those reported by other authors on samples of similar length [6,7,29]. The observed differences reflect the average increased rigidity experienced by two successive base pairs which oppose the rotational motion of the molecules.

The rms average fluctuation of the torsion angle $\langle \Delta\xi \rangle$ between adjacent base pairs in DNA can be obtained by the relation [30]:

$$\langle \Delta\xi \rangle = \sqrt{\frac{k_B T}{\alpha}}$$

where h is the distance between base pairs equal to 3.4×10^{-8} cm; k_B, the Boltzman constant, is 1.38×10^{-16} erg K^{-1}; T, the absolute temperature is 283 K and α, the torsional constant is 4.2×10^{-12} and 4.7×10^{-12} erg for the control and the 'scrambled' samples, respectively. Applying this expression we obtain a 0.29°/base pairs higher value of $\langle \Delta\xi \rangle$ for the control sample; for a 27-mer fragment this means an overall increase in the twist angle of 7.5° for the less rigid control sample as compared to the 'scrambled' one. This value corresponds to a 0.8% increase in the total twist of our samples, assumed to be in a conventional B-form, where the twist angle is equal to approximately 36° per each base pair. We stress the high sensitivity of the FPA measurements to detect minor differences in the mean torsion of the DNA.

The increase of melting temperature and torsional constant in the 'scrambled' sample are consistent with an increase of stacking energy between base pairs. We think that further systematic experimental and theoretical studies should be desirable using well characterized samples both in composition and in length. The availability of DNA samples in which a fluorescent base could allow monitoring of internal motion, at a well defined position, will improve the understanding of this correlation, attributing the real rigidity value to each dinucleotide pair.

Acknowledgements

This work was partially supported by CNR. We are grateful to Giberto Chirico for providing the software for fluorescence polarization anisotropy data fitting and for the helpful discussion. We wish to thank Paola Di Ciaccio for her help in editing the manuscript.

References

[1] H.M. Berman, W.K. Olson, D.L. Beveridge, et al., Biophys. J. 63 (1992) 751.
[2] L. Bossi, D.M. Smith, Cell 39 (1984) 643.
[3] A. Nordheim, E.M. Lafer, L.J. Peck, J.C. Wang, B.D. Stollar, A. Rich, Cell 31 (1982) 309.
[4] S. Neidle, Nature Struct. Biol. 5 (1998) 754.
[5] J.M. Schurr, Chem. Phys. 84 (1984) 71.
[6] M. Collini, G. Chirico, G. Baldini, M.E. Bianchi, Biopolymers 36 (1995) 211.
[7] J. Duhamel, J. Kanyo, G. Dinter-Gottlieb, P. Lu, Biochemistry 35 (1996) 16687.
[8] F. Barone, G. Chirico, M. Matzeu, F. Mazzei, F. Pedone, Eur. Biophys. J. 27 (1998) 137.
[9] J.S. Sun, T. Garestier, C. Helene, Curr. Opin. Struct. Biol. 3 (1996) 345.
[10] J. Franchet-Beuzit, M. Spotheim-Maurizot, B. Sabattier, B. Blazy Baudras, M. Charlier, Biochemistry 32 (1993) 2104.
[11] F. Barone, M. Belli, F. Mazzei, Radiat. Environ. Biophys. 33 (1994) 23.
[12] J. Sambrook, E.F. Fritsch, T. Maniatis, Molecular Cloning, A Laboratory Manual, Spring Harbor Laboratory Press, Cold Spring Harbor, NY, 1989.
[13] C.R. Cantor, M.M. Warshaw, H. Shapiro, Biopolymers 9 (1970) 1059.
[14] K.J. Breslauer, in: S. Agrawal (Ed.), Protocols for Oligonucleotides Conjugates (Methods in Molecular biology, vol. 26). Humana Press Inc, Totowa NJ, 1994, pp. 347–372.
[15] S.A. Allison, J.M. Schurr, Chem. Phys. 41 (1979) 35.
[16] M.M. Tirado, J. Garcia de la Torre, Chem. Phys. 73 (1980) 1986.
[17] S.S. Chan, K.J. Breslauer, M.E. Hogan, et al., Biochemistry 29 (1990) 6161.
[18] H.C. Nelson, J.T. Finch, B.F. Luisi, A. Klug, Nature 330 (1987) 221.
[19] J. Aymami, M. Coll, C.A. Frederick, A.H. Wang, A. Rich, Nucleic Acid Res. 17 (1989) 3229.
[20] W.D. Henner, S.M. Grunberg, W.A. Haseltine, J. Biol. Chem. 257 (1982) 11750.
[21] D. Sy, C. Savoye, M. Begusova, V. Michalik, M. Charlier, M. Spotheim-Maurizot, Int. J. Radiat. Biol. 72 (1997) 147.
[22] R. Negri, G. Costanzo, E. Di Mauro, Anal. Biochem. 197 (1991) 389.
[23] D.M. Crothers, T.E. Haran, J.G. Nadeau, J. Biol. Chem. 265 (1990) 7093.
[24] M. Kochoyan, J.L. Leroy, Curr. Opin. Struct. Biol. 5 (1995) 329.

[25] T.D. Tullius, in: F. Eckstein, D.M.J. Lilley (Eds.), Structural Studies of DNA Trough Cleavage by the Hydroxyl Radical (Nucleic Acids and Molecular Biology, vol. 3), Springer, Berlin, Heidelberg, New York, 1992, pp. 1–12.
[26] R.E. Dickerson, H.R. Drew, J. Mol. Biol. 149 (1981) 761.
[27] N. Sugimoto, S. Nakano, M. Yoneyama, K. Honda, Nucleic Acid Res. 24 (1996) 4501.
[28] J. SantaLucia, Proc. Natl. Acad. Sci. USA 95 (1998) 1460.
[29] B.S. Fujimoto, J.M. Miller, N.S. Ribeiro, J.M. Schurr, Biophys. J. 67 (1994) 304.
[30] M.D. Barkley, B.H. Zimm, J. Chem. Phys. 70 (1979) 2991.